Magnetic phase diagrams of the ferromagnetic Kondo lattice $CePd_2Al_8$

Le Wang,[1,2,3] Cuixiang Wang,[1,2,3] Ziyi Liu,[1,4] Jinguang Cheng,[1,3,5] Shanshan Miao,[1] Youting Song,[1] Youguo Shi,[1,2,3,5,*] and Yi-feng Yang[1,3,5,†]

[1]*Beijing National Laboratory for Condensed Matter Physics, Institute of Physics, Chinese Academy of Sciences, Beijing 100190, China*

[2]*Center of Materials Science and Optoelectronics Engineering, University of Chinese Academy of Sciences, Beijing 100049, China*

[3]*School of Physical Sciences, University of Chinese Academy of Sciences, Beijing 100190, China*

[4]*Department of Physics, Harbin Institute of Technology, Harbin 150001, China*

[5]*Songshan Lake Materials Laboratory, Dongguan, Guangdong 523808, China*

(Received 7 March 2019; revised manuscript received 24 July 2019; published 12 August 2019)

We report the synthesis and detailed investigation of the single crystal $CePd_2Al_8$. Resistivity measurements reveal typical metallic behavior at high temperatures and a plateau at about 15 K followed by a rapid drop due to successive antiferromagnetic (AFM) and ferromagnetic (FM) transitions. The specific heat and magnetic susceptibility present obvious anomalies related to both transitions. We find an extremely large magnetic anisotropy with $\chi_a/\chi_b > 2000$ at 2 K. With increasing magnetic field, the AFM transition temperature is gradually suppressed and only the ferromagnetic phase remains above 500 Oe for $H \parallel a$, with an ordered moment of 1.43 μ_B, while for $H \parallel b$ the FM transition turns into an AFM-like transition. With pressure, the two phases merge at 12.5 GPa into a possibly ferromagnetic phase, pointing to a possible critical point at higher pressures. We construct the temperature-magnetic field and temperature-pressure phase diagrams for the single crystal $CePd_2Al_8$.

DOI: 10.1103/PhysRevB.100.085122

I. INTRODUCTION

In heavy fermion materials, exotic electronic states often occur near magnetic phase boundaries and their properties may be very different depending on the nature of their associated magnetic long-range orders [1–3]. For antiferromagnetic (AFM) compounds such as $CeIn_3$ [4], $CeRhIn_5$ [5], and $YbRh_2Si_2$ [6], a magnetic quantum critical point (QCP) can often be approached by (chemical) pressure or magnetic field, giving rise to either d-wave superconductivity or unusual quantum critical behaviors. For ferromagnetic (FM) compounds such as UGe_2 [7–9], superconductivity has been reported under pressure with possible spin-triplet pairing. However, unlike its AFM counterpart, a ferromagnetic quantum phase transition is typically missing, interrupted either by other phases or a sudden collapse (first order) of the magnetism. Theoretical analysis based on itinerant ferromagnetism excludes the FM QCP at zero field in clean materials and points to a first order FM phase transition in general, although it was recently claimed to exist in the quasi-one-dimensional Kondo lattice $YbNi_4(P_{1-x}As_x)_2$ [10,11], and another compound, $CeRh_6Ge_4$, was also argued to be in proximity to a FM QCP [12]. However, compared to the many AFM families, FM compounds are very few in number and therefore less studied. Their syntheses, especially single crystal samples of high quality, may provide new opportunities for revealing the richness of heavy fermion physics.

Recently, a new Ce-based intermetallics, $CePd_2Al_8$, was reported [13] to adopt a totally new monoclinic structure and form a ferromagnetic order at 9.5 K in the polycrystal. To explore the physics of its ferromagnetism, we have successfully synthesized the $CePd_2Al_8$ single crystal and carried out systematic physical properties measurements. Our data revealed two successive magnetic transitions (AFM and FM) at low temperatures and a moderately enhanced specific heat coefficient in the normal state. Applying a magnetic field suppresses the AFM and drives the system into a single FM phase. We find a large magnetic anisotropy for field along the a and b axis and observe a large ordered moment of 1.43 μ_B along the easy a axis. Under pressure, both magnetic phases are enhanced at first but then suppressed and merge into a single phase of most probably FM nature at about 12.5 GPa, pointing to potential suppression of FM and related physics at higher pressures in this new class of Kondo lattice compounds.

II. EXPERIMENTAL DETAILS

Single crystals of $CePd_2Al_8$ were grown using an Al self-flux method. The starting materials were mixed in a molar ratio of 1:2:30 in a glovebox filled by argon. The mixture was placed in an alumina crucible sealed in a fully evacuated quartz tube. The crucible was heated to 1120 °C for 15 h, then cooled slowly to 700 °C at 2 K/h, where the flux was centrifuged. Large shiny single crystals were yielded with the volume of about 0.5 mm × 0.3 mm × 2.5 mm as shown in the inset of Fig. 1(d). The excess Al flux was removed by the diluted NaOH solution. Single crystal x-ray diffraction was carried out on a Bruker D8 Venture diffractometer at 273(2) K using Mo Kα radiation ($\lambda = 0.71073$ Å). The

*ygshi@iphy.ac.cn
†yifeng@iphy.ac.cn

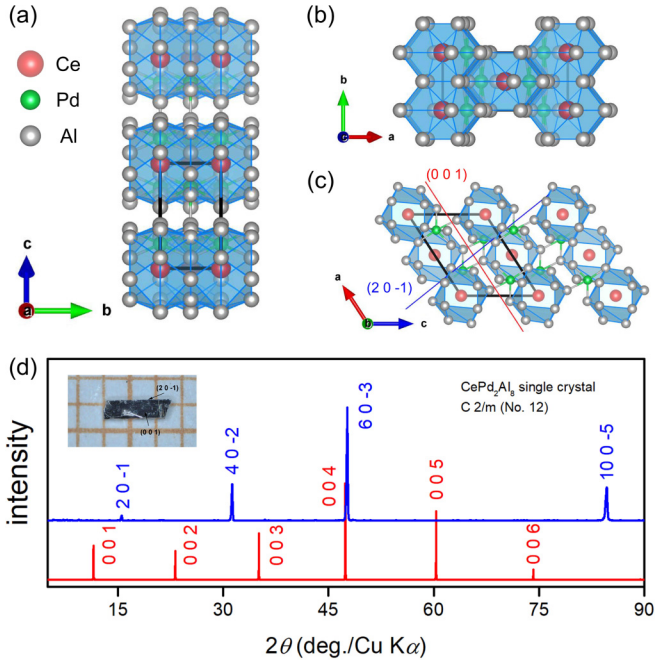

FIG. 1. Projection of the crystal structure of $CePd_2Al_8$ onto the *bc* plane (a), *ab* plane (b), and *ac* plane (c). The black solid line indicates one unit cell. The red ball denotes Ce atom, the green ball denotes Pd atom, and the gray ball denotes Al atom. (d) XRD patterns of the single crystal measured on the (0 0 1) and (2 0 −1) surfaces in (c).

crystal structure was refined by full-matrix least-squares fitting on F^2 using the SHELXL-2014/7 program. Surface indexation of the crystal was studied by x-ray diffraction (XRD) on a Rigaku Smartlab High Resolution Diffractometer at room temperature using Cu $K\alpha_1$ radiation ($\lambda = 1.5406$ Å). Elemental analysis was conducted via energy dispersive x-ray (EDX) spectroscopy using a Hitachi S-4800 scanning electron microscope at an accelerating voltage of 15 kV, with an accumulation time of 90 s. The result of EDX indicated the stoichiometric composition of $CePd_2Al_8$. A well crystallized sample was picked out for the measurements. The specific heat (C_p) and electrical resistivity (ρ) were measured in a physical property measurement system (PPMS) between 2 and 300 K, using a thermal-relaxation method and a standard dc four-probe technique, respectively. The magnetic susceptibility (χ) was measured in a Quantum Design magnetic property measurement system (MPMS) between 2 and 300 K with various applied magnetic fields along the *a* and *b* axis in field-cooling (FC) and zero-field-cooling (ZFC) modes. The high-pressure resistivity up to 12.5 GPa was measured with the standard four-probe method by using the palm cubic anvil cell (CAC) apparatus. Details about the experimental setup can be found elsewhere [14,15]. Glycerol has been employed as the pressure transmitting medium and the pressure values were determined at room temperature by observing the characteristic phase transitions of bismuth and lead.

III. RESULTS AND DISCUSSION

As examined by single crystal x-ray diffraction, $CePd_2Al_8$ has a different structure from that of previously known 128 family such as $CeCo_2Ga_8$ [16]. The results are summarized in Tables I and II. It adopts a monoclinic structure with the space group $C2/m$ and the lattice parameters, $a = 11.4799(6)$ Å, $b = 4.4269(2)$ Å, $c = 9.1398(4)$ Å, and $\beta = 123.145(2)^\circ$, which are consistent with previously published data [13]. The smaller values of R (1.84%) and wR_2 (4.55%) suggest that our single crystals are of high quality. As illustrated in Figs. 1(a)–1(c), it is formed of Ce-centered $CeAl_{14}$ cages packed along the *b* axis with sharing faces and along the *a* axis with sharing edges. The crystal is of high purity and the XRD data in

TABLE I. Crystallographic data of $CePd_2Al_8$.

empirical formula	$CePd_2Al_8$
formula weight	568.76 g/mol
temperature	273(2) K
wavelength	Mo K_α (0.71073 Å)
crystal system	monoclinic
space group	$C2/m$ (12)
unit cell dimensions	$a = 11.4799(6)$ Å
	$b = 4.4269(2)$ Å
	$c = 9.1398(4)$ Å
	$\beta = 123.145(2)^\circ$
cell volume	388.91(3) Å^3
Z	2
density, calculated	4.857 g/cm^3
$h\ k\ l$ range	$-15 \leqslant h \leqslant 15$
	$-5 \leqslant k \leqslant 5$
	$-12 \leqslant l \leqslant 12$
$2\theta_{max}$	56.644
linear absorption coeff.	11.135 mm^{-1}
absorption correction	multiscan
no. of reflections	4264
T_{min}/T_{max}	0.616/0.746
R_{int}	0.0192
no. independent reflections	545
no. observed reflections	521 [$F_o > 4\sigma(F_o)$]
$F(000)$	508
R values	1.84 % ($R_1[F_o > 4\sigma(F_o)]$)
	4.55 % (wR_2)
weighting scheme	$w = 1/[\sigma^2(F_o^2) + (0.00254P)^2$
	$+1.1107P]$,
	where $P = (F_o^2 + 2F_c^2)/3$
diff. Fourier residues	[−2.431, 1.008] e/Å^3
refinement software	SHELXL-2014/7

TABLE II. Atomic coordinates and equivalent isotropic thermal parameters of $CePd_2Al_8$.

Site	WP[a]	x	y	z	U_{eq}	OP[b]
Ce	2a	0	0	0	0.005395(11)	1
Pd	4i	0.19333(3)	0	0.76877(4)	0.005898(11)	1
Al1	4i	0.62220(14)	0	0.29620(17)	0.007084(2)	1
Al2	4i	0.06726(14)	0	0.41364(17)	0.008317(3)	1
Al3	4i	0.29804(14)	0	0.36937(16)	0.007231(3)	1
Al4	4i	0.33993(13)	0	0.10189(16)	0.006792(3)	1

[a]Wyckoff position.
[b]Occupation.

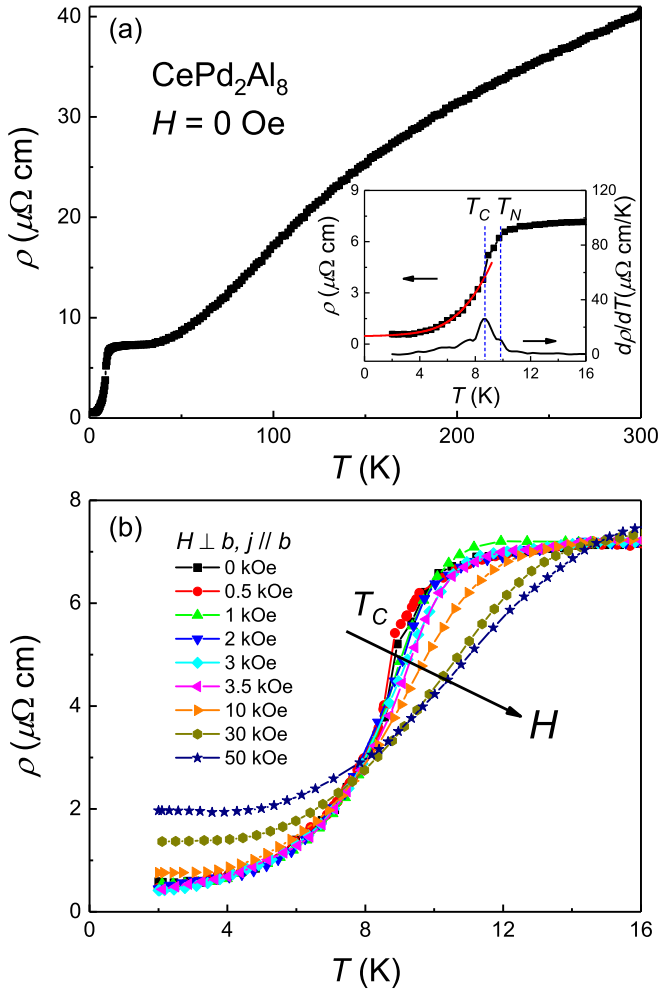

FIG. 2. (a) Temperature dependence of the electrical resistivity for $CePd_2Al_8$. Inset: rapid decrease of the resistivity at low temperatures, showing two kinks due to the antiferromagnetic (T_N) and ferromagnetic (T_C) transitions. (b) Low temperature variations of the electrical resistivity of $CePd_2Al_8$ with magnetic field perpendicular to the b axis.

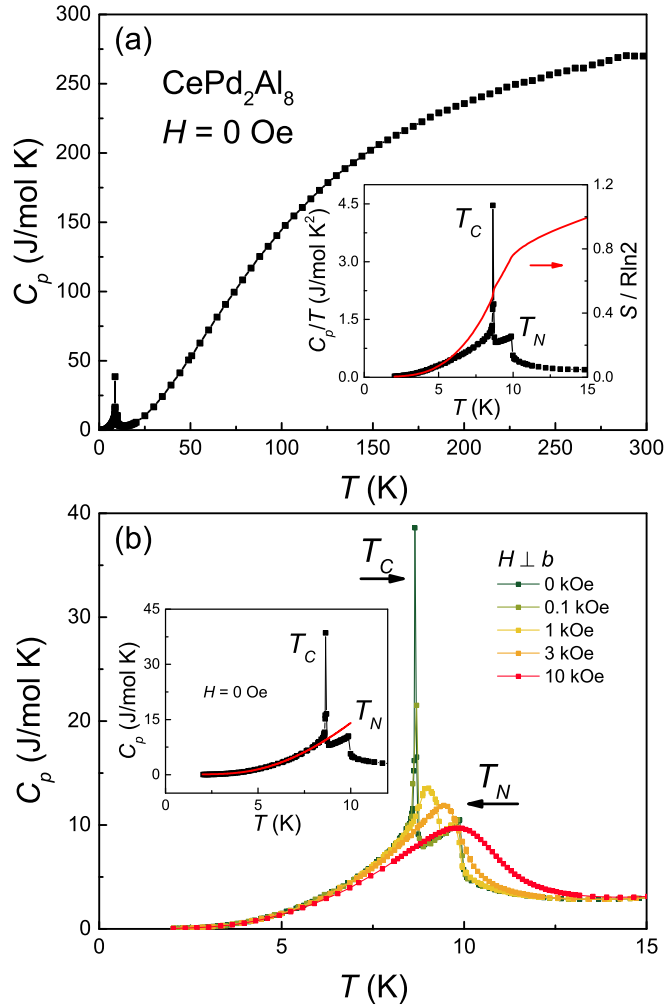

FIG. 3. (a) Temperature dependence of the zero-field specific heat for $CePd_2Al_8$. Inset: C_p/T with two clear anomalies corresponding to the AFM and FM transitions, respectively, and the derived entropy S as a function of temperature. (b) Evolution of the AFM and FM transitions in specific heat with magnetic field perpendicular to the b axis. The inset shows the enlarged plot, in which the red line is a linear fit to the low temperature data at zero field.

Fig. 1(d) show no visible impurity peaks. We have identified the two flat surfaces as the (0 0 1) and (2 0 −1) planes.

Figure 2 plots the temperature dependence of the electrical resistivity $\rho(T)$ for $CePd_2Al_8$. The metallic behavior of the resistivity at above 50 K may be attributed to the electron-phonon scattering. Below 50 K, one sees a plateau with a weak maximum at about 15 K, followed by a rapid decrease of the resistivity below about 10 K. While the plateau may be attributed to a combined effect of the Kondo and phonon contributions and indicates the presence of incoherence Kondo scattering, the rapid decrease of the resistivity is associated with two successive AFM and FM transitions. This is roughly indicated by $d\rho/dT$ plot in the inset but will become evident below in the specific heat and susceptibility data. The two magnetic transitions are very close. A weak shoulder was also present but ignored in a previous report on polycrystalline samples [13]. This indicates that our single crystal is of high quality. The residual resistivity at 2 K is 0.46 $\mu\Omega$ cm, yielding a large residual resistivity ratio (RRR), $\rho(300K)/\rho(2K) \approx 85$. Below T_C, the resistivity can be well fitted with the expression,

$$\rho(T) = \rho_0 + AT^2 + DT\Delta^{-1}(1 + 2T\Delta^{-1})e^{-\Delta/T}, \quad (1)$$

where ρ_0 is the residual resistivity, the second term is the Fermi liquid contribution, and the third term originates from the magnon scattering in the ferromagnet [17]. The coefficient D reflects the electron-magnon coupling and Δ represents the gap in the magnon dispersion. Our best fit yields $A = 0.0125\ \mu\Omega\,\mathrm{cm/K^2}$, $\rho_0 = 0.482\ \mu\Omega\,\mathrm{cm}$, and $\Delta = 2.3$ meV. In Fig. 2(b), a magnetic field was applied up to 50 kOe. We see that the transitions in the electrical resistivity become smooth and the residual resistivity is enhanced. As we will see below, applying the magnetic field suppresses T_N and enhances T_C, driving the system to a single FM phase above 3.5 kOe.

The magnetic transitions are most evidently seen in the specific heat data. Figure 3 plots the temperature and field

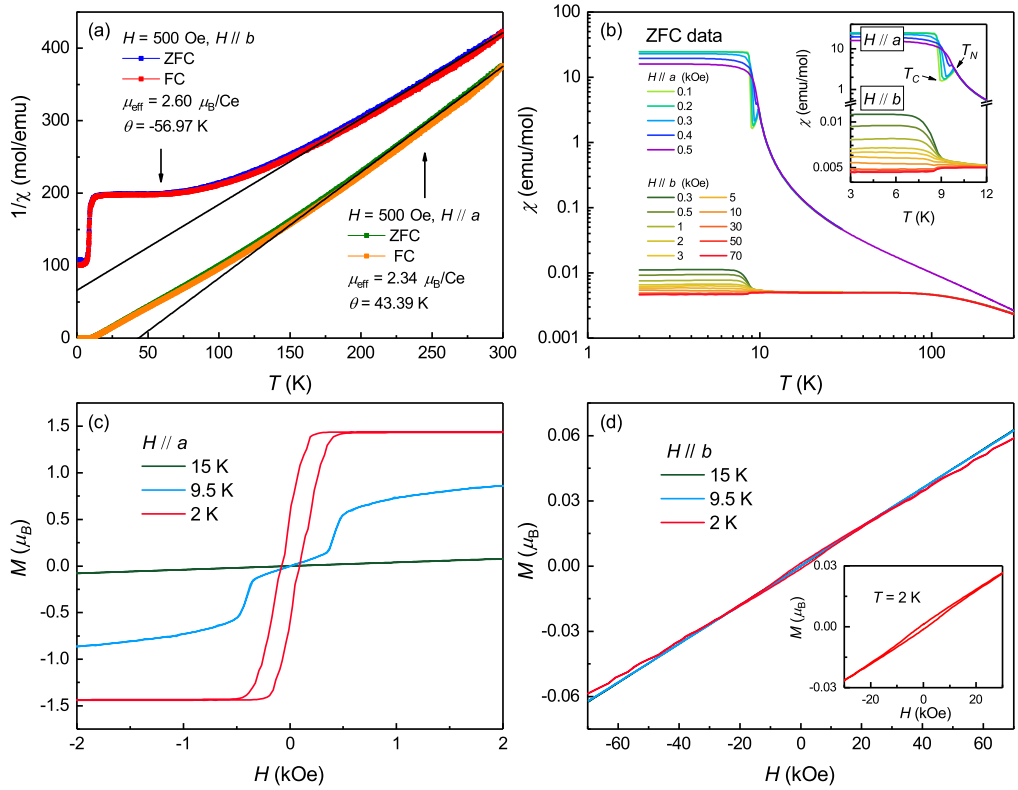

FIG. 4. (a) Temperature dependence of the ZFC and FC inverse susceptibility for $CePd_2Al_8$ with a magnetic field of 500 Oe parallel to the a axis and b axis, respectively. The black solid line is the fit with the Curie-Weiss law. (b) The ZFC susceptibility under various magnetic field $H \parallel a$ and $H \parallel b$. The inset shows T_C defined as the onset of the rapid upturn and T_N as the onset of the sharp decrease. (c),(d) The isothermal magnetization at $T = 2$, 9.5, 15 K for $H \parallel a$ and $H \parallel b$, respectively.

dependence of the specific heat for $CePd_2Al_8$. At 300 K, C_p is about 269.9 J/mol K, close to the Dulong-Petit limit [18], $3nR = 274.4$ J/mol K, where $n = 11$ is the total number of atoms per formula unit and R is the gas constant. Two sharp λ-type anomalies are clearly observed at $T_N \approx 9.8$ K and $T_C \approx 8.7$ K, with an entropy release of $0.8R \ln 2$ at T_N. The jump at T_C is much larger and sharper than that at T_N in zero field, suggesting dominant ferromagnetic correlation at low temperatures. The entropy, $S(T)$, exhibits distinct changes in slope at both transitions and reaches $R \ln 2$ at about 15 K. The latter indicates a doublet ground state of the Ce $4f$ electrons and, together with the resistivity maximum at roughly the same temperature, implies a coherence temperature of $T^* \approx 15$ K, below which the f-electron spins start to entangle (hybridize) with conduction electrons to form heavy quasiparticles and release its magnetic entropy [19,20].

In the ferromagnetic state below T_C, the specific heat data may be fitted using

$$C_p = \gamma T + B(\Delta^2/\sqrt{T} + 3\Delta\sqrt{T} + 5T^{3/2})e^{-\Delta/T}, \quad (2)$$

where γ is the specific heat coefficient of hybridized quasiparticles and the second term describes the magnon contribution [21]. As shown in the inset of Fig. 3(b), an excellent fit was obtained between 2 K and 8 K, yielding $\gamma = 52$ mJ/mol K^2 and $\Delta = 1.9$ meV. The moderately enhanced γ implies the presence of partially hybridized f-electron states. We obtain a Kadowaki-Woods ratio, $A/\gamma^2 \approx 0.462 \times 10^{-5}$ μΩ cm (mol K mJ^{-1})^2, which is comparable with those of other heavy-fermion compounds [22]. The derived magnitude of Δ is also consistent with that estimated from the resistivity fit, supporting the opening of a magnetic gap below T_C. The magnetic field dependence of the specific heat is shown in Fig. 3(b). While the transition at T_C is shifted to higher temperatures and becomes a broad crossover, the anomaly at T_N is gradually suppressed to lower temperatures. These confirm the FM and AFM nature of the two transitions, respectively. Above 3.5 kOe, T_N is suppressed into the ferromagnetic phase, but no anomaly is observed below T_C, indicating that the AFM is taken over by a single polarized FM phase at high field.

The AFM and FM nature of the two transitions can be further confirmed by the susceptibility measurement. Figures 4(a) and 4(b) plot the temperature dependence of the inverse susceptibility $1/\chi$ and the susceptibility χ measured with field along the crystallographic a and b axis. At high temperatures, one can obtain excellent Curie-Weiss fits using $\chi = C/(T - \theta)$, which yields the Curie constant $C = 0.684$ emu K/mol, the Weiss temperature $\theta = 43.39$ K for $H \parallel a$ and $C = 0.848$ emu K/mol, $\theta = -56.97$ K for $H \parallel b$. The resulting effective moments, $\mu_{\text{eff}} = 2.34\ \mu_B$ ($H \parallel a$) and $2.60\ \mu_B$ ($H \parallel b$), are both close to the theoretical value, $2.54\ \mu_B$, of a free Ce^{3+} ion. The different sign of θ along two directions indicates that the magnetic correlations are ferromagneticlike along the a axis and antiferromagneticlike along the b axis. Below 10 K, χ_a exhibits a small peak at the AFM transition, and then increases sharply to a nearly

T-independent value at slightly lower temperatures, marking the transition into a polarized FM state. With increasing magnetic field, the AFM transition is quickly suppressed. By contrast, for the field along the b axis, only the FM transition is seen at low field, which turns into an AFM-like transition at higher field. We observe an extremely large magnetic anisotropy developing at low temperatures, with the ratio χ_a/χ_b increasing from the order of unity above 300 K to over 2000 at 2 K. The origin of such a huge magnetic anisotropy remains to be investigated. We should note that due to the large anisotropy, a tiny misalignment of the sample would yield a significant contribution to the measured χ_b. We cannot fully exclude this possibility, although we have carefully aligned the sample to minimize this effect. On the other hand, the absence of successive AFM and FM transitions in χ_b in Fig. 4(b) seems to support its intrinsic nature.

To further confirm the nature of these magnetic transitions, we have measured the isothermal magnetization at 2, 9.5, 15 K as shown in Figs. 4(c) and 4(d). The M-H curves exhibit different behaviors for field along the a and b axes. For $H \parallel a$, the magnetization increases linearly with field at 15 K as expected for a paramagnetic state. At 9.5 K, the linear field dependence only appears below 350 Oe and is interrupted by a step at about 500 Oe, indicating the possibility of a spin-flip transition. At 2 K, the magnetization saturates at 500 Oe and exhibits a typical hysteresis loop for a ferromagnet. For $H \parallel b$, $M(H)$ at 15 K and 9.5 K are both linear with the field and a tiny hysteresis loop shows up at 2 K with the coercivity of about 2 kOe, showing no saturation at high field. More interestingly, we can see a weak quantum oscillation pattern above 2 kOe. A detailed analysis of the oscillation might help to reveal the Fermi surface properties of the compound. We obtain the magnetic moments of 1.43 μ_B at 500 Oe (saturated) for $H \parallel a$ and 0.06 μ_B at 70 kOe (unsaturated) for $H \parallel b$, confirming the easy a axis and the large magnetic anisotropy. These results have been examined in several other samples and may also be compared with the reported value of 0.89 μ_B in polycrystalline samples [13]. The transition temperatures, T_C and T_N, may be defined by the successive downturn and upturn of $\chi(T)$ with lowering temperatures, respectively. The two transitions at T_C and T_N for $H \parallel a$ merge together at about 9.5 K and 500 Oe with increasing field, as shown in the susceptibility data. Since there exists no additional features below the FM transition, the antiferromagnetic order appears to be completely suppressed above the critical field of about 500 Oe. A temperature-magnetic field (T-H) phase diagram of $CePd_2Al_8$ can be constructed as shown in Fig. 5, which includes three separate regions corresponding to the high-temperature paramagnetic (PM) phase, the low-temperature FM phase and the intermediate AFM phase.

To explore the possible existence of FM QCP, we have also measured the electrical resistivity $\rho(T)$ for $CePd_2Al_8$ single crystal under hydrostatic pressures up to 12.5 GPa by using the palm cubic anvil cell. The data are summarized in Fig. 6(a). Both magnetic transitions are seen in the derivative curves $d\rho/dT$ in Fig. 6(b). With increasing pressure, T_N and T_C increase initially, but then decrease above 4 GPa until they eventually merge together at 12.5 GPa, where only one anomaly can be discerned. It is noteworthy that the resistivity

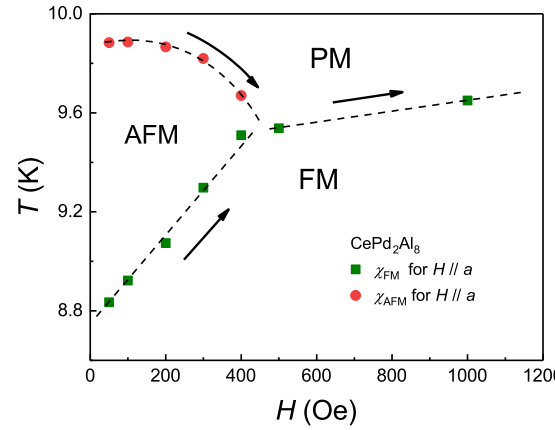

FIG. 5. Temperature-magnetic field (T-H) phase diagram of $CePd_2Al_8$ based on the magnetic susceptibility data for $H \parallel a$. The dashed lines and arrows are guides to the eyes.

right above the magnetic transitions experiences a significant reduction above 10 GPa, whose origin also deserves further investigations. The resulting temperature-pressure phase diagram is plotted in the inset of Fig. 6(a). Unfortunately, we have not achieved full suppression of the magnetic orders. From the overall pressure dependence of the peaks in $d\rho/dT$, we expect that the high pressure transition is ferromagnetic. However, confirmative evidences for its FM nature and possible existence of FM QCP or superconductivity can only be examined in future measurements at higher pressures.

IV. CONCLUSION

The magnetic phase diagrams of the Kondo-lattice material $CePd_2Al_8$ has been investigated with a magnetic field up to 70 kOe or an external pressure up to 12.5 GPa by means of electrical resistivity, specific heat, and magnetic

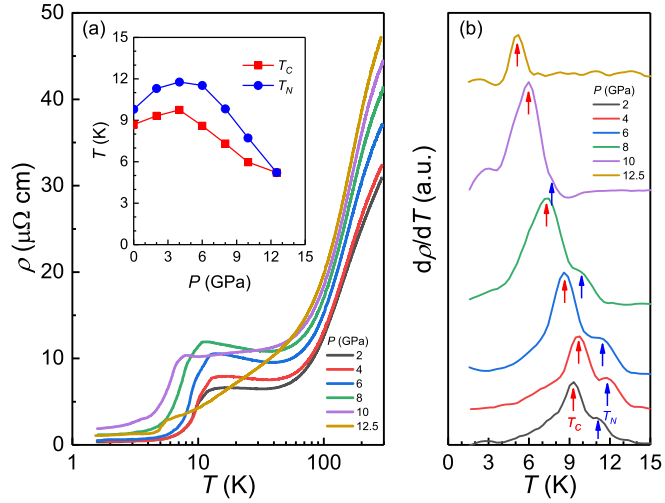

FIG. 6. (a) Temperature dependence of the resistivity for $CePd_2Al_8$ single crystal under pressure. Inset: the pressure dependence of T_N and T_C. (b) The first-order derivative of $\rho(T)$, showing clear signatures of both transitions marked by the arrows.

susceptibility measurements. We find that $CePd_2Al_8$ undergoes two successive transitions at zero field, an AFM transition at 9.8 K, and a FM transition at 8.7 K. The two phases merge together above 500 Oe for field along the *a* axis or pressure above 12.5 GPa. The high-field or high-pressure phase is most probably ferromagneticlike. This provides a material basis for future exploration of potential ferromagnetic quantum criticality or superconductivity in $CePd_2Al_8$. By contrast, only the FM transition is observed for $H \parallel b$ at low field, which turns into an AFM-like transition at high field. Interestingly, a huge magnetic anisotropy is seen to develop at low temperatures with the magnetic ratio, χ_a/χ_b, exceeding 2000. Thus $CePd_2Al_8$ could be a candidate low-dimensional magnetic system whose origin and implications are worthy of further exploration.

ACKNOWLEDGMENTS

This work was supported by the National Key R&D Program of China (Grants No. 2017YFA0302901, No. 2017YFA0303103, No. 2016YFA0300604, No. 2018YFA0305702), the National Natural Science Foundation of China (NSFC Grants No. 11522435, No. 11774399, No. 11774401, No. 11574377), the State Key Development Program for Basic Research of China (Grants No. 2015CB921300), the Chinese Academy of Sciences (CAS) (No. QYZDB-SSW-SLH043, No. QYZDB-SSW-SLH013), the Beijing Natural Science Foundation (Z180008), the National Youth Top-notch Talent Support Program of China, the Youth Innovation Promotion Association of CAS, and the K. C. Wong Education Foundation (GJTD-2018-01).

[1] B. D. White, J. D. Thompson, and M. B. Maple, Physica C **514**, 246 (2015).
[2] F. Steglich and S. Wirth, Rep. Prog. Phys. **79**, 84502 (2016).
[3] O. Stockert and F. Steglich, Annu. Rev. Condens. Matter Phys. **2**, 79 (2011).
[4] G. Knebel, D. Braithwaite, P. C. Canfield, G. Lapertot, and J. Flouquet, Phys. Rev. B **65**, 024425 (2001).
[5] T. Park, F. Ronning, H. Q. Yuan, M. B. Salamon, R. Movshovich, J. L. Sarrao, and J. D. Thompson, Nature (London) **440**, 65 (2006).
[6] J. Custers, P. Gegenwart, C. Geibel, F. Steglich, P. Coleman, and S. Paschen, Phys. Rev. Lett. **104**, 186402 (2010).
[7] S. S. Saxena, P. Agarwal, K. Ahilan, F. M. Grosche, R. K. W. Haselwimmer, M. J. Steiner, E. Pugh, I. R. Walker, S. R. Julian, P. Monthoux, G. G. Lonzarich, A. Huxley, I. Sheikin, D. Braithwaite, and J. Flouquet, Nature (London) **406**, 587 (2000).
[8] A. Huxley, I. Sheikin, E. Ressouche, N. Kernavanois, D. Braithwaite, R. Calemczuk, and J. Flouquet, Phys. Rev. B **63**, 144519 (2001).
[9] N Tateiwa, T. C. Kobayashi, K. Hanazono, K. Amaya, Y. Haga, R. Settai, and Y. Ōnuki, J. Phys.: Condens. Matter **13**, 6443 (2001).
[10] C. Krellner, S. Lausberg, A. Steppke, M. Brando, L. Pedrero, H. Pfau, S. Tencé, H. Rosner, F. Steglich, and C. Geibel, New J. Phys. **13**, 103014 (2011).
[11] A. Steppke, R. Küchler, S. Lausberg, E. Lengyel, L. Steinke, R. Borth, T. Lühmann, C. Krellner, M. Nicklas, C. Geibel, F. Steglich, and M. Brando, Science **339**, 933 (2013).
[12] E. Matsuoka, C. Hondo, T. Fujii, A. Oshima, H. Sugawara, T. Sakurai, H. Ohta, F. Kneidinger, L. Salamakha, H. Michor, and E. Bauer, J. Phys. Soc. Jpn. **84**, 073704 (2015).
[13] A. Tursina, E. Khamitcaeva, D. Gnida, and D. Kaczorowski, J. Alloys Compd. **731**, 229 (2018).
[14] J.-G. Cheng, K. Matsubayashi, S. Nagasaki, A. Hisada, T. Hirayama, M. Hedo, H. Kagi, and Y. Uwatoko, Rev. Sci. Instrum. **85**, 093907 (2014).
[15] J.-G. Cheng, B.-S. Wang, J.-P. Sun, and Y. Uwatoko, Chin. Phys. B **27**, 077403 (2018).
[16] L. Wang, Z. Fu, J. Sun, M. Liu, W. Yi, C. Yi, Y. Luo, Y. Dai, G. Liu, Y. Matsushita, K. Yamaura, L. Lu, J.-G. Cheng, Y.-F. Yang, Y. Shi, and J. Luo, npj Quantum Mater. **2**, 36 (2017).
[17] V. A. Sidorov, E. D. Bauer, N. A. Frederick, J. R. Jeffries, S. Nakatsuji, N. O. Moreno, J. D. Thompson, M. B. Maple, and Z. Fisk, Phys. Rev. B **67**, 224419 (2003).
[18] C. Kittel, *Introduction to Solid State Physics* (Wiley, New York, 1966).
[19] Y.-F. Yang, Z. Fisk, H. O. Lee, J. D. Thompson, and D. Pines, Nature (London) **454**, 611 (2008).
[20] Y.-F. Yang, Rep. Prog. Phys. **79**, 074501 (2016).
[21] B. Coqblin, *The Electronic Structure of Rare-Earth Metals and Alloys: The Magnetic Heavy Rare-Earths* (Academic, New York, 1977).
[22] K. Kadowaki and S. B. Woods, Solid State Commun. **58**, 507 (1986).